

Comparison of electron cyclotron heating results in the helically symmetric experiment with and without quasi-symmetry

To cite this article: K M Likin *et al* 2003 *Plasma Phys. Control. Fusion* **45** A133

View the [article online](#) for updates and enhancements.

You may also like

- [Ion-temperature-gradient stability near the magnetic axis of quasisymmetric stellarators](#)

R Jorge and M Landreman

- [Neoclassical plasma viscosity and transport processes in non-axisymmetric tori](#)

K.C. Shaing, K. Ida and S.A. Sabbagh

- [Radial electric field and ion parallel flow in the quasi-symmetric and Mirror configurations of HSX](#)

S T A Kumar, T J Dobbins, J N Talmadge et al.

Comparison of electron cyclotron heating results in the helically symmetric experiment with and without quasi-symmetry

K M Likin¹, A Abdou¹, A F Almagri¹, D T Anderson¹, F S B Anderson¹, D Brower², J Canik¹, C Deng², S P Gerhardt¹, W Guttenfelder¹, S Oh¹, J Radder¹, V Sakaguchi¹, J Schmitt¹, J Tabora¹, J N Talmadge¹ and K Zhai¹

¹ The HSX Plasma Laboratory, University of Wisconsin-Madison, USA

² Electrical Engineering Department, University of California, Los Angeles, USA

Received 11 July 2003

Published 10 November 2003

Online at stacks.iop.org/PPCF/45/A133

Abstract

The extraordinary wave at the second harmonic of the electron cyclotron frequency produces and heats the plasma in the helically symmetric experiment. Ray-tracing calculations predict 40% first pass absorption at a plasma density of $1.5 \times 10^{18} \text{ m}^{-3}$ and an electron temperature of 400 eV. To measure the wave absorption, a set of absolutely calibrated microwave detectors is installed along the machine. It was found that the absorption efficiency is very high (about 0.9) in the quasi-helically symmetric (QHS) and mirror configurations, and it drops to 0.6 in the anti-mirror mode. The confinement of particles in the different configurations is studied in the neutral gas breakdown experiments. With the same gas pressure and heating power, the density for the QHS configuration has a larger growth rate (10^4 s^{-1}) compared with the mirror ($5 \times 10^3 \text{ s}^{-1}$) and anti-mirror modes ($2 \times 10^3 \text{ s}^{-1}$). A study of the stored energy versus launched power and plasma density shows that it increases linearly (up to 50 J) with power and has a maximum at a low plasma density (at about $0.4 \times 10^{18} \text{ m}^{-3}$). The central electron temperature measured by Thomson scattering also rises linearly with heating power and reaches 600 eV at 100 kW of launched power.

1. Introduction

The quasi-helically symmetric (QHS) magnetic configuration in the helically symmetric experiment (HSX) has a helical axis of symmetry in contrast to conventional stellarators, which have no symmetry at all. In conventional stellarators the asymmetry in the magnetic ripple causes a large deviation of the particle trajectory from a flux surface, direct loss orbits and large transport at low collisionality. Restoring the axis of symmetry to a stellarator leads to improved neoclassical confinement in the low collisionality regime and neoclassical transport comparable

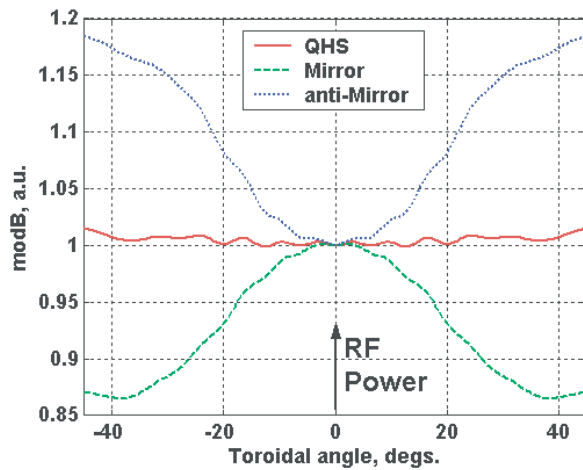


Figure 1. Mod $|B|$ along the plasma axis in QHS, mirror and anti-mirror configurations.

with that of a tokamak [1]. Unlike a conventional stellarator, the toroidal curvature term in the HSX magnetic field spectrum has been shown to be negligibly small and the dominant spectral component is helical with a poloidal mode number $m = 1$ and toroidal mode number $n = 4$ [2]. The 48 modular coils produce the quasi-helical magnetic field. So-called mirror configurations in HSX are produced with auxiliary coils in which an additional toroidal mirror term is added to the magnetic field spectrum. In the mirror configuration the mirror term is added to the main field at the location of the launching antenna, and in the anti-mirror mode it is opposite to the main field. The magnitude of the magnetic field along the axis for the QHS, mirror and anti-mirror configurations, as well as the resonance location, are shown in figure 1. The mirror configurations reproduce the neoclassical transport of a conventional stellarator. Thus, by varying the currents in the auxiliary coils, we are able to study plasma confinement with and without quasi-symmetry in this machine. The HSX major radius is 1.2 m, the average plasma minor radius is 0.15 m and the plasma volume is about 0.44 m^3 [3]. The plasma build-up and heating in HSX is done at a magnetic field of 0.5 T using the extraordinary wave at the second harmonic of the electron cyclotron frequency. The microwave power (up to 100 kW so far at 28 GHz) is launched from the low magnetic field side in the form of a Gaussian beam focused at the plasma centre with a spot size of 4 cm.

In this paper, recent results on neutral gas breakdown, X-wave absorption, stored energy and central electron temperature in different magnetic configurations are reported.

2. Neutral gas breakdown

The particle confinement properties in different magnetic configurations of HSX are studied in the experiments on neutral gas breakdown. Breakdown time, growth rate and plasma density peak are measured as a function of (1) the cyclotron resonance location, (2) the gas pressure inside the vacuum vessel and (3) the RF electric field strength. Because the wave beam is well focused, the RF field in front of the antenna is very high: at 40 kW of launched power, the local RF field strength is 1.5 kV cm^{-1} . The linear theory of X-wave—electron interaction at the second harmonic predicts zero absorption in a ‘cold’ plasma. Nonetheless, neutral gas ionization by X-wave at the second harmonic was observed in the first generation stellarators with RF heating, for instance, in heliotron-E and Wendelstein-7A [4, 5]. The model by Carter

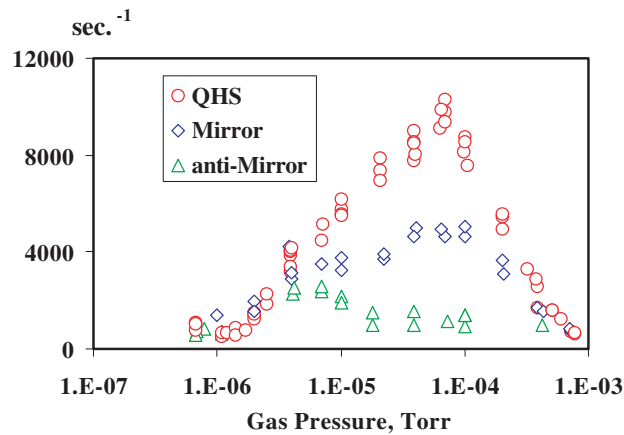


Figure 2. Growth rate versus gas pressure in QHS, mirror and anti-mirror ($P_{in} = 40$ kW).

claims that due to a non-linear interaction between the wave and deeply trapped electrons, such particles can undergo perpendicular energy excursions that are larger than the ionization potential [6].

In the experiment on neutral gas breakdown, the vacuum vessel is filled with hydrogen through a needle valve. At a fixed flow rate, the gas pressure inside the HSX remains constant. To reduce the breakdown time (the time interval between the start of the heating pulse and the ionization avalanche), the population of the seed electrons in the vacuum vessel is increased with a filament and/or UV flash lamp. The plasma density growth rate is determined from an exponential fit to the central chord signal of the interferometer.

In the magnetic field scan it was found that the maximum growth rate in each magnetic configuration occurs when the cyclotron resonance is on the magnetic axis. A scan in neutral gas pressure has been made at central resonance with 40 kW of launched power (figure 2). The growth rate in all configurations is small at a gas pressure less than 10^{-6} Torr and higher than 10^{-3} Torr. At a very low gas pressure ($<10^{-6}$ Torr) there is no difference between the magnetic configurations because the number of ionizing electrons is not sufficient to produce an avalanche, and at a high gas pressure the electrons cannot gain enough energy in the RF field due to frequent collisions with neutrals. In the range 4×10^{-6} – 4×10^{-4} Torr, effective ionization of neutral gas takes place. A competition between the acceleration of electrons in a strong RF field, atomic physics processes (collisions with neutrals, electron impact ionization, dissociation) and particle confinement leads to the formation of a maximum in the growth rate. In the QHS mode, the maximum growth rate is higher by a factor of 2 as compared with that in the mirror mode. In the anti-mirror configuration, the confinement of deeply trapped electrons is so poor that the growth rate is very low and almost independent of the gas pressure.

By varying the injection power, one can understand how the RF electric field affects the plasma density growth rate. The growth rate drops and its maximum is shifted to the low gas pressure when the power launched into the vacuum vessel is decreased (figure 3). The role of the local RF field strength is also demonstrated in experiments with ordinary mode injection into the torus. The polarization is changed by rotating the TE_{01} – HE_{11} mode converter in the waveguide transmission line. The O-wave beam waist is not changed. Hence, for the same injected power level, the RF field in front of the antenna remains the same as in the X-mode experiments, but the effective RF field strength drops because the O-mode has a very low

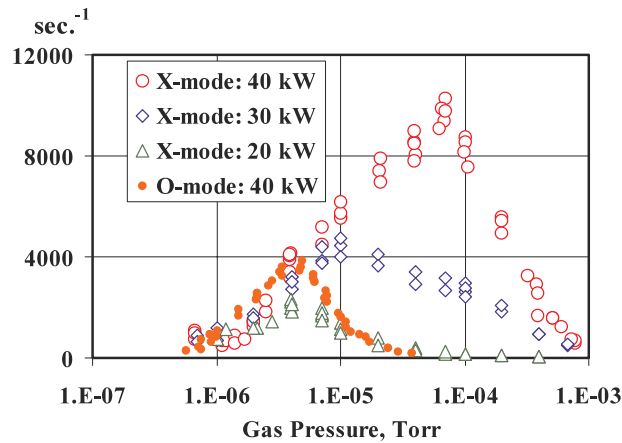


Figure 3. Growth rate for X-wave at different injected power levels and O-wave at 40 kW in the QHS configuration.

absorption efficiency at the second harmonic. Because of reflections from the vessel wall, the O-mode is converted into an X-polarized wave, which causes the gas to breakdown. Due to the reduced effective RF field, the growth rate decreases (see figure 3).

3. Extraordinary wave absorption in HSX

Ray-tracing codes are used to estimate the absorption for the first pass of the microwave power through the plasma column [7]. One can also extend the calculations to the fraction of the injected power that is not absorbed in the first pass [8]. To simulate the propagation of the electron cyclotron waves in HSX plasma, the standard geometric optics equations and the cold plasma refractive index are used [9]. The local absorption coefficient is evaluated taking into consideration a finite temperature [10]. The power in each ray is weighted in accordance with a Gaussian form of the incident wave (the beam radius is 2 cm at the e^{-2} power level). The magnetic field components are calculated using the Biot–Savart method. In typical runs of the code, a parabolic plasma density profile, $n \sim (1 - r^2)$, and an exponential electron temperature profile, $T \sim \exp(-2r^2)$, are used, where r is the effective plasma radius. To find the effective plasma radius, a linear interpolation over 16 radial, 50 poloidal and 51 toroidal data points uniformly distributed over the nested flux surfaces is used.

In the experiment, the absorption efficiency and the local deposition of microwave energy along the torus can be determined with a set of microwave antennae [11]. On HSX, six absolutely calibrated microwave detectors are installed at different distances from the microwave power antenna. The location of the microwave detectors around the machine is as follows. The antennae #1, #2, #3 and #4 are mounted counterclockwise in the toroidal direction at 6.3° , 36° , 69.3° and 103° with respect to the heating power launch port. Antennae 3 and 5, and 4 and 6 are installed symmetrically with respect to the launch port. Each antenna consists of an open-ended rectangular waveguide, attenuator and microwave detector. The E -plane of the rectangular waveguide antennas is oriented perpendicular to the magnetic field so that mostly X-wave power is detected. The antennas can be rotated in order to measure the waves with an arbitrary polarization. The signals from the microwave detectors are amplified with a gain of about 30 and collected by the data acquisition system.

After a few reflections from the wall one can expect the microwave power to be isotropic, and the non-absorbed power can be estimated from the following expression:

$$P_{\text{non}} = \frac{U \cdot S_i \cdot S_v}{G_i \cdot Wg \cdot Att \cdot \text{trs}_w}$$

where U is the acquired signal; G_i , amplifier gain; S_i , diode sensitivity; Att , attenuation coefficient; trs_w , transparency of quartz window; Wg , effective area of waveguide antenna; S_v , area of cross-section perpendicular to the helical axis inside the vacuum chamber at diode location. We define the multi-pass absorption coefficient as $\eta = 1 - P_{\text{non}}/P_0$, where P_{non} is the measured non-absorbed power and P_0 is a reference power, which in this case is the power measured for a ‘cold’ plasma discharge when the plasma density was above the cut-off.

3.1. Results of ray-tracing calculations

Calculations of ray trajectories at the HSX box port where the ECH antenna is located show that the ray refraction is small because the wave propagates almost along the plasma density and magnetic field gradients. At a central electron temperature of 0.4 keV, the single-pass absorption coefficient is 0.4 at a line average density of $1.5 \times 10^{18} \text{ m}^{-3}$ and rises linearly with plasma density up to the cut-off at $3 \times 10^{18} \text{ m}^{-3}$ [12]. Also shown in figure 4 is the single-pass absorption coefficient as a function of plasma density using the central electron temperature measured by Thomson scattering.

We consider the problem of estimating the multi-pass absorption in the following manner. Power that is not absorbed in the first pass is reflected from the vacuum vessel wall and back into the plasma in the form of a wide, divergent beam. Considering the stainless steel wall on the inward side of the HSX vacuum vessel as a mirror, the reflected beam radius is estimated to be 6 cm with a 20° divergence. The total absorption for two passes reaches as high as 70% at a density of $2 \times 10^{18} \text{ m}^{-3}$ and 400 eV central electron temperature. The absorbed power profile does not significantly broaden when multi-pass absorption is considered (figure 5).

3.2. Results of measurements

The multi-pass absorption efficiency versus the plasma density in QHS and mirror configurations is shown in figure 6 (only four detectors are shown, #1, #2, #3 and #4, while the

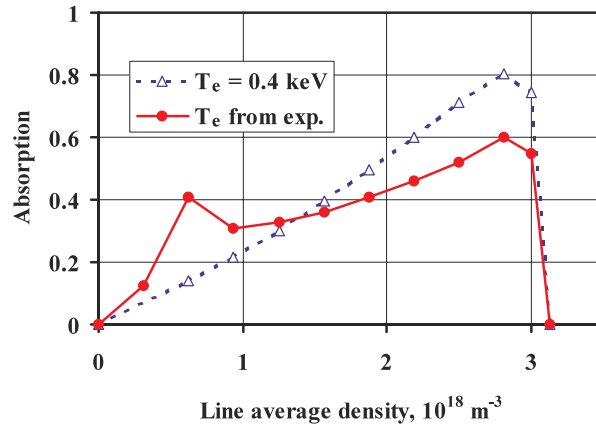


Figure 4. Single-pass absorption versus line average plasma density.

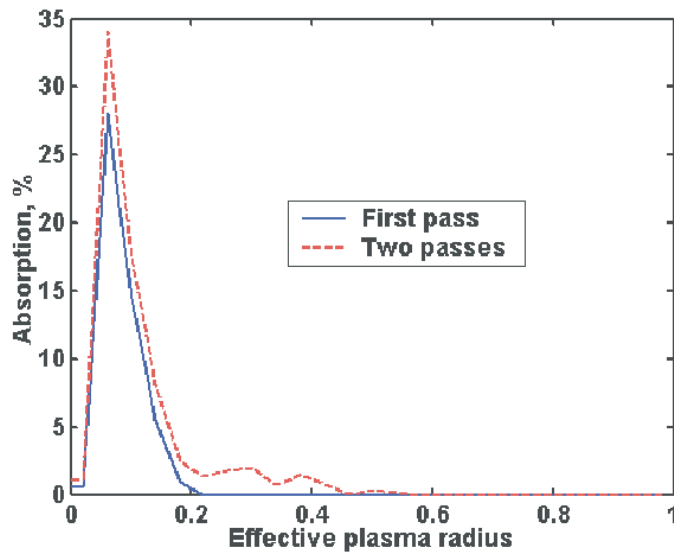


Figure 5. Absorption profiles: $B_0 = 0.5$ T; $N_e = 2 \times 10^{18} \text{ m}^{-3}$; $T_e(0) = 0.4$ keV.

detectors #5 and #6 measure the same power level as #3 and #4). From the figure it can be seen that the absorption is localized near the launch antenna (note that antenna #1 is only 18 cm away from it); i.e. most power is absorbed in a few passes through the plasma column. At a low plasma density ($< 0.5 \times 10^{18} \text{ m}^{-3}$), the absorption drops in the mirror mode, while it remains high in the QHS configuration. In the anti-mirror configuration the electron temperature is low (the stored plasma energy is only 5–7 J), and the multi-pass absorption efficiency does not exceed 0.6. In this configuration, the electron cyclotron heating drastically increases the number of deeply trapped electrons in the local magnetic well and they leave the confinement volume in a short time because they are on direct loss orbits [13].

Another method to determine the absorbed power is based on an evaluation of the change in slope of the diamagnetic loop signal before and after the heating power turn-off. In all regimes of HSX operation, the values obtained with this technique are 50% of the launched power or less. One possible reason for the discrepancy between the microwave detector measurement and the diamagnetic loop is the high losses due to radiation, recombination, charge exchange and absorption on super-thermal electrons.

4. Plasma stored energy studies

The stored energy in HSX is measured with the diamagnetic loop mounted inside the vacuum vessel [14]. The plasma density profile is measured by a microwave interferometer and the electron temperature by one-channel Thomson scattering as well as by a four-channel ECE radiometer. Measurements of the stored energy have been made as a function of the plasma density and the launched power in different magnetic configurations.

In the launched power scan, we varied the power from 20 to 100 kW. The stored energy and the central electron temperature rise linearly with the power in both QHS and mirror configurations (figures 7 and 8). The radiated power also goes up linearly with launched power and is roughly 50% of the absorbed power estimated from the diamagnetic loop slope. There is no real difference observed in the QHS and mirror energy confinement. This is consistent

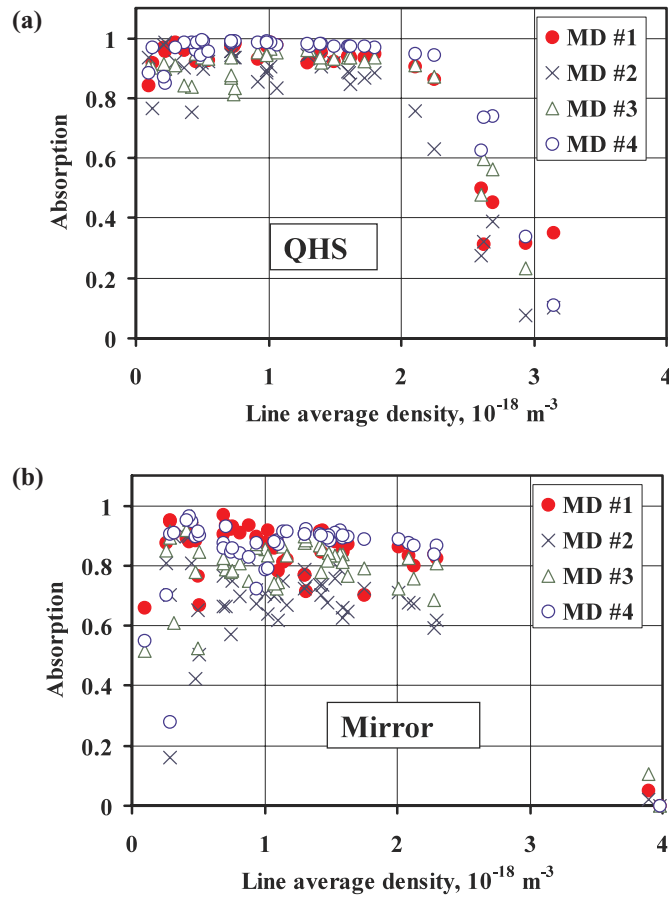


Figure 6. Multi-pass absorption coefficient measured by microwave detectors: (a) QHS mode; (b) mirror mode.

with calculations using the one-dimensional ASTRA code, which includes a calculation of the ambipolar electric field [15]. The mono-energetic diffusion coefficient is calculated using a Monte-Carlo code. With zero electric field, the neoclassical thermal conductivity is at least two to three orders of magnitude higher in the mirror mode than in the QHS configuration. In the ASTRA calculation, the electron thermal conductivity is assumed to be a sum of the neoclassical contribution and an anomalous term. With the inclusion of the electric field in the neoclassical model, the neoclassical terms for both the mirror and QHS configurations at a magnetic field of 0.5 T and 20 kW of absorbed power are small compared with the anomalous contribution. In contrast, at 1.0 T and 100 kW absorbed power, the code predicts a 200–300 eV difference in the central electron temperature.

At a density of $0.4 \times 10^{18} \text{ m}^{-3}$, the stored energy has a maximum (figure 9). The central electron temperature measured by Thomson scattering increases by a factor of 2 at the low density in the QHS configuration as compared with that at the high plasma density (figure 10), while the central ECE signals increase by a factor of 4. The high emission measured by ECE and the hard x-ray detector at the low plasma density is probably due to a population of super-thermal electrons. It is necessary to measure the electron energy spectrum for accurate interpretation of the Thomson scattering results.

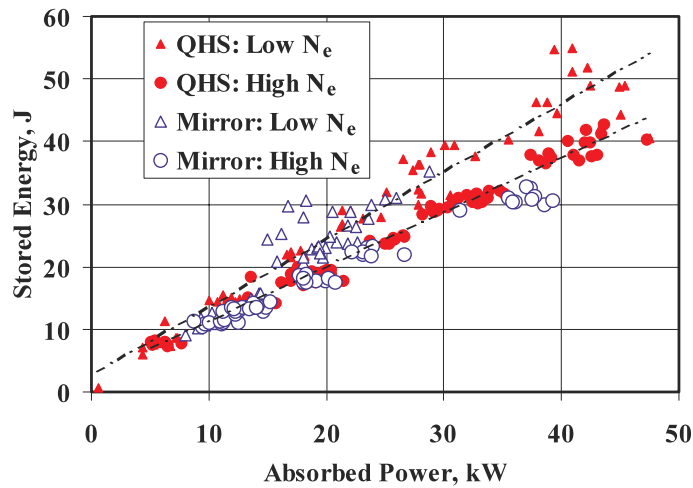


Figure 7. Stored energy versus the absorbed power at a low plasma density ($0.5 \times 10^{18} \text{ m}^{-3}$) and at a high density ($1.5 \times 10^{18} \text{ m}^{-3}$).

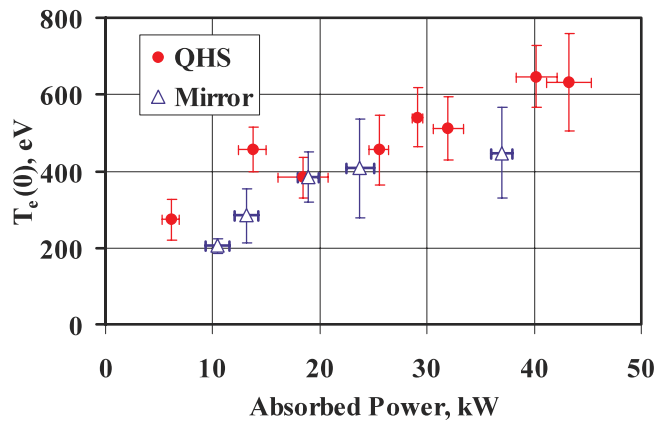


Figure 8. Central electron temperature as a function of absorbed power.

It was found that the plasma stored energy strongly depends on the fuelling. This phenomenon is distinct at the low plasma density (about $0.5 \times 10^{18} \text{ m}^{-3}$); for instance, the stored energy can be almost double in some regimes. The stored energy is enhanced when the source of gas fuelling is further away from the plasma axis. The enhancement is probably due to an increase of the super-thermal electron population. When the puffing valve is moved further away from the plasma axis, the neutral density drops in the plasma centre, where the resonant RF–electron interactions take place. This idea is supported by neutral density measurements and numerical modelling. Electrons then gain more energy between collisions because they suffer less scattering on neutrals. The neutral density is measured by an array of 16 H_α detectors. Nine detectors are installed at one toroidal location, and another seven detectors monitor the toroidal variation of the light. The experimental data on H_α emission are in good agreement with results of DEGAS code calculations [16]. In HSX, the three-dimensional DEGAS code predicts a flat atomic hydrogen profile and molecular hydrogen concentration that is localized to the immediate vicinity of the gas feed.

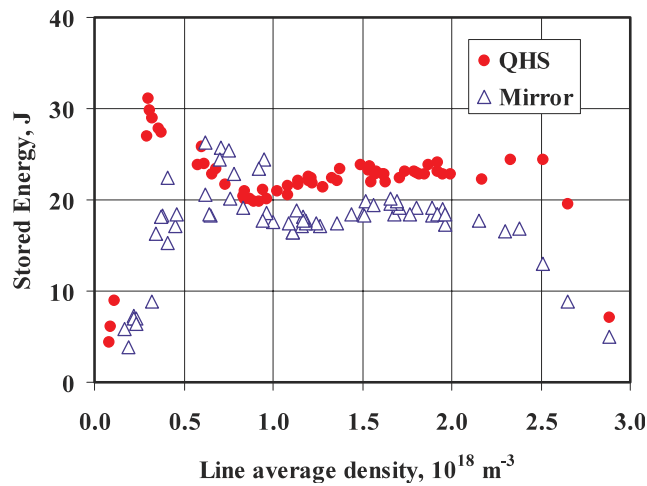


Figure 9. Stored energy versus plasma density ($P_{in} = 40$ kW).

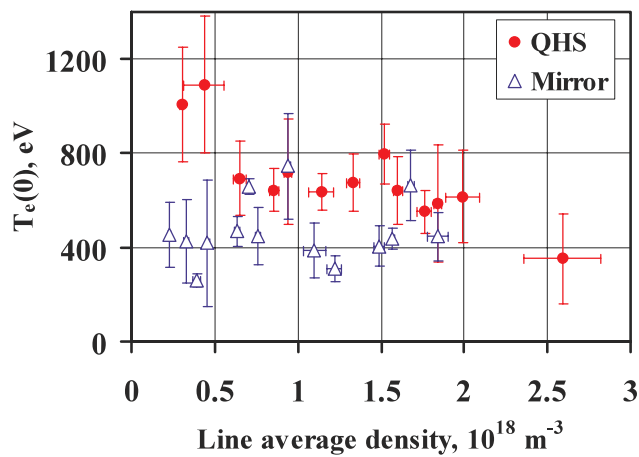


Figure 10. Central electron temperature as a function of plasma density ($P_{in} = 40$ kW).

5. Summary

Plasma growth rates measured during neutral gas breakdown clearly indicate a difference in particle confinement for three magnetic configurations. In the QHS mode, the plasma density rises twice as fast (10^4 s^{-1}) as in the mirror configuration, while the growth rate in the anti-mirror plasma is substantially smaller, $2 \times 10^3 \text{ s}^{-1}$.

In the QHS and mirror modes, the extraordinary wave at the second harmonic is absorbed with high efficiency (0.9) in a few passes through the plasma column. Owing to the high electron temperature measured by Thomson scattering and a population of super-thermal electrons observed by both the ECE and hard x-ray detectors, the absorption remains high at a low plasma density. The multi-pass absorption should be taken into account in ray-tracing calculations in order to get a reasonable agreement with the results of the measurements. In the anti-mirror configuration, the multi-pass absorption is poor (0.6) because of the low electron temperature and poor confinement of trapped particles.

There is no real difference observed in the stored energy and the electron temperature for QHS and mirror discharges at 0.5 T magnetic field and up to 100 kW input power. The transport due to anomalous thermal conductivity dominates over the neoclassical losses. In the anti-mirror configuration the particle direct orbit losses significantly degrade the heating efficiency. At a high plasma density ($1.5 \times 10^{18} \text{ m}^{-3}$) the energy confinement time is about 1 ms and the central electron temperature measured by Thomson scattering is in excess of 600 eV for both the QHS and mirror configurations.

Acknowledgment

The work is supported by DOE grant #DE-FG02-93ER54222.

References

- [1] Nührenberg J and Zille R 1988 Quasi-helically symmetric toroidal stellarators *Phys. Lett. A* **129** 113–17
- [2] Talmadge J N, Sakaguchi V, Anderson F S B, Anderson D T and Almagri A F 2001 Experimental determination of the magnetic field spectrum in the helically symmetric experiment using passing particle orbits *Phys. Plasmas* **8** 5165
- [3] Anderson F S B, Almagri A F, Anderson D T, Mathews P G, Talmadge J N and Shohet J L 1995 The helically symmetric experiment (HSX) goals, design and status *Fusion Technol.* **27** 273
- [4] Uo K *et al* 1985 Neutral beam injection and RF heating experiments on the currentless plasma in heliotron E *Plasma Phys. Control. Nucl. Fusion Res.* **2** 383
- [5] Erckmann V 1986 Electron cyclotron resonance heating in the Wendelstein VII-A *Plasma Phys. Control. Fusion* **28** 1277–90
- [6] Carter M D, Batchelor D B and England A C 1987 Second harmonic electron cyclotron breakdown in stellarators *Nucl. Fusion* **27** 985–96
- [7] Likin K M and Ochirov B D 1991 Ray tracing and absorption of microwaves in connection with electron cyclotron resonance heating of the plasma in the L-2 stellarator *Sov. J. Plasma Phys.* **18** 42–6
- [8] Goldfinger R C and Batchelor B D 1989 Numerical model for electron cyclotron heating profiles in stellarator geometry *Nucl. Fusion* **29** 1743–9
- [9] Stix T H 1992 *Waves in Plasmas* (New York: Springer) pp 69–87
- [10] Alikaev V V, Litvak A G, Suvorov E V and Friman A A 1992 Electron cyclotron heating of plasma in toroidal devices *High-Frequency Plasma Heating* ed A G Litvak (New York: American Institute of Physics) pp 3–14
- [11] Batanov G M *et al* 1991 Absorption of microwaves in connection with ECR heating of the plasma in the L-2 stellarator *Sov. J. Plasma Phys.* **18** 33–8
- [12] Likin K M *et al* 2003 Absorption of X-wave at the second harmonic in HSX *15th Conf. on RF Power in Plasmas (Moran WY, USA, 2003)* (American Institute of Physics) submitted
- [13] Gerhardt S P *et al* 2002 Experimental evidence for improved confinement with quasisymmetry in HSX *19th Int. Conf. on Plasma Phys. and Control. Nucl. Fusion (Lyon, France, 2002)* IAEA-CN-94/EX/P3-22
- [14] Almagri A F, Anderson D T, Deng C, Gerhardt S P and Talmadge J N 2002 Plasma thermal energy dependence on field ripple and direct orbit losses *13th Int. Stellarator Workshop (Canberra, Australia, March 2002)*
- [15] Talmadge J N *et al* 2002 Transport in HSX electron cyclotron heated plasmas at 0.5 T *13th Int. Stellarator Workshop (Canberra, Australia, March 2002)*
- [16] Heifetz D B 1986 Neutral particle transport *Physics of Plasma–Wall Interactions in Controlled Fusion* ed D E Post and R Behrisch (New York: Plenum) pp 695–771